U-Pb isotopic dating of titanite microstructures: Potential implications for the chronology and identification of large impact structures

K. Papapavlou[1*], J. R. Darling[2], D. E. Moser[3], I. R. Barker[3], EIMF[4], L. F. White[5], P. C. Lightfoot[3], C. D. Storey[2], J. Dunlop[2]

[1]GEOTOP, Université du Québec à Montréal, Montréal, Québec, H2X 3Y7, Canada
[2]School of Earth and Environmental Sciences, University of Portsmouth, Portsmouth, PO1 3QL, UK
[3]Department of Earth Sciences, University of Western Ontario, London, Ontario, N6A 5B7, Canada
[4]Edinburgh Ion Microprobe Facility, School of Geosciences, Grant Institute, University of Edinburgh, EH9 3JW, UK
[5]Department of Natural History, Royal Ontario Museum, Toronto, Ontario, M5S 2C6, Canada

*e-mail address of corresponding author: constantinepapapavlou@gmail.com

Abstract

Identifying and dating large impact structures is challenging, as many of the traditional shock indicator phases can be modified by post-impact processes. Highly robust accessory phases, such as zircon, while faithful recorders of shock wave passage, commonly respond with partial U-Pb age resetting during impact events. Titanite is an accessory phase with lower Pb closure temperature than many other robust chronometers, but its potential as indicator and chronometer of impact-related processes remains poorly constrained. In this study, we examined titanite grains from the Sudbury (Ontario, Canada) and Vredefort (South Africa) impact structures, combining quantitative microstructural and U-Pb dating techniques. Titanite grains from both craters host planar microstructures and microtwins that show a common twin-host disorientation relationship of 74° about <102>.In the Vredefort impact structure, the microtwins deformed internally and developed high and low-angle grain boundaries that resulted in the growth of neoblastic crystallites. U-Pb isotopic dating of magmatic titanite grains with deformation microtwins from the Sudbury impact structure yielded a $^{207}Pb/^{206}Pb$ age of 1851 ± 12 Ma that records either the shock heating or the crater modification stage of the impact event. The titanite grains from the Vredefort impact structure yielded primarily pre-impact ages recording the cooling of the ultra-high temperature Ventersdorp event but domains with microtwins or planar microstructures show evidence of U-Pb isotopic disturbance. Despite that the identified microtwins are not diagnostic of shock-metamorphic processes, our contribution demonstrates that titanite has great potential to inform studies of the terrestrial impact crater record.

Keywords: Titanite, Sudbury, Vredefort, U-Pb geochronology, EBSD, Impact craters

Introduction

U and Th-bearing accessory phases, such as zircon ($ZrSiO_4$), monazite ((LREE) PO_4), and baddeleyite (ZrO_2), show increasing potential as recorders and chronometers of impact bombardment (Krogh et al., 1984, Moser, 1997, Cavosie et al., 2015, Darling et al., 2016, Erickson et al., 2016, White et al., 2018). The high closure temperature for Pb diffusion of these phases (zircon T_c = > 900°C, Cherniak and Watson, 2000; baddeleyite T_c = > 900°C, Heaman and Lecheminant, 2000; monazite T_c = 700 to > 800°C; Parrish, 1990) means that the majority of shock deformed and annealed grains preserve a largely undisturbed age of protolith crystallization (Abramov et al., 2013).

Titanite ($CaTiSiO_5$) is another widely occurring accessory mineral (Frost et al., 2001) that may contain significant concentrations of U (up to 1000 ppm), and most importantly has a lower closure temperature to Pb diffusion (~ 650 °C for a cooling rate of 10°C/Ma; Cherniak, 1993) than the aforementioned U-Th-Pb chronometers. In addition, it has also been reported from a wide range of planetary materials such as lunar breccia deposits (Grieve et al., 1975), ultramafic ureilites (Guan and Crozaz, 2000), and Vesta-derived eucrites (Delaney et al., 1983), as well as terrestrial crustal rocks from the Eoarchaean to present day.

Despite the presence of titanite within shocked meteorites and target rocks associated with terrestrial impact craters (e.g. Sudbury, Vredefort, and Manicouagan craters) the potential of titanite as a shock indicator and chronometer of impact bombardment remains poorly understood. Previous attempts to date an impact event with titanite proved successful in Manicouagan impact crater using U-Th/He isotope systematics (Van Soest et al., 2011). However, U-Pb age dating of pre-impact titanite grains yielded pre-impact ages with no evidence of age resetting by the impact heating (Biren and Spray., 2011, M. Biren, 2017, personal communication).

In order to further our understanding about the potential of titanite, we adopt in this study the approach of microstructural geochronology, combining quantitative microstructural analysis (Electron Backscatter Diffraction; EBSD) and high-spatial resolution geochronology (Secondary Ion Mass Spectrometry; SIMS). The main aims of this study are to: (a) quantitatively document and subsequently date titanite microstructures found in grains associated with the Sudbury and Vredefort craters, (b) evaluate the potential of this abundant accessory phase as a recorder and chronometer of impact-related processes, and (c) better constrain the role of deformation twinning on age resetting.

Background information on crystallography and microstructures in titanite ($CaTiSiO_5$)

Titanite is a monoclinic ($P2_1/a$), orthosilicate mineral, that exhibits simple growth twinning on {100} and occasionally lamellar mechanical twinning on {221} crystallographic planes (Deer et al, 1997). Titanite accommodates crystal-plastic strain with the development of dislocation creep microstructures (i.e. high and low-angle grain boundaries, strain-free neoblasts) and deformation twins (Muller and Franz.,2004, Spencer et al., 2013, Bonamici et al., 2014, Bonamici et al., 2015, Papapavlou et al., 2017). Specifically, deformation twins have been described in titanite grains associated with tectonic and shock metamorphic processes (Borg, 1970, Stoffler, 1972, Langenhorst and Dressler., 2003, Bonamici et al., 2015). Generally, twinning can develop: (a) by the presence of lattice defects during the growth of a crystal (growth twins), (b) during phase transformations, such as space group shifts (transformation twins), and (c) by the application of shear stresses on a crystal (deformation twins) (Putnis, 1992). Deformation twins commonly have tapering morphology, variable width, and they often overprint and deform previous generations of twins (Vernon, 2004).

Titanite undergoes high-temperature and high-pressure phase transitions resulting from the displacement of the Ti^{4+} atoms within its corner-sharing TiO_6 octahedra (Kunz et al., 1996). In more detail, a reversible displacive phase transition is observed in titanite at 220 ± 20° C, from the primitive $P2_1/a$ to orthorhombic A2/a space group, but the development of transformation twins has not been reported (Taylor and Brown.,1976, Ghose et al., 1991). Titanite grains retrieved from artificially shocked granitoids during nuclear detonation events (P = 1.4 – 1.8 GPa) and grains experimentally deformed under static conditions (P=0.8 GPa, T = 25 – 500°C, $e = 10^{-5}$ S^{-1}) show the development of two sets of twins that intersect each other at 55 ± 2° (Borg and Heard.,1972). The twin glide system in these grains is characterised by the following elements (terminology based on Christian and Mahajan., 1995): K1 (twin or slip plane) = {221} with η1 (slip direction) = [110] and K2 = {-131} with η2 = irrational (Borg., 1970). Moreover, the deformation twins reported in Borg., 1970 show a disorientation relationship of 180°/<110> and are characterised as type 2 twins sensu Christian and Mahajan., 1995). Experimental shock loading of titanite grains up to ~59 GPa produced reduction of birefringence, intense mosaicism, and development of polycrystalline aggregates with a minimal effect on the U-Pb age resetting of the examined grains (Deutsch and Scharer, 1990). Moreover, titanite grains within shocked anorthositic rocks, from the central uplift of the Late Triassic Manicouagan impact crater, exhibit partial melting, deformed mechanical twins, and planar microstructures (Biren and Spray., 2010, Biren and Spray., 2011).

Geological setting and sample description

The Sudbury impact structure

The 1850 ± 2 Ma Sudbury impact structure (Ontario, Canada) is located between the Neoarchean Superior and Paleoproterozoic Southern provinces (Krogh et al., 1984; Lightfoot, 2017). The original diameter of the Sudbury crater is estimated to be 200 – 250 km, with the structure divided into the South, East and North Range (Riller., 2005; **Fig. 1A**). The three main lithostratigraphic units of the crater are: (a) the Sudbury Igneous Complex (SIC) that comprises a differentiated impact melt sheet, (b) the impact produced pseudotachylitic Sudbury breccia, and (c) the Onaping Formation of the Whitewater group that comprises volcanosedimentary and fallback deposits (Ames et al., 2000). The Sudbury structure is bounded at the South Range by metamorphosed volcaniclastic rocks of the Huronian Supergroup and at the North Range by the Neoarchean tonalitic gneisses of the Levack gneiss complex (Lightfoot, 2017). The Sudbury structure underwent metamorphism in greenschist up to epidote-amphibolite facies conditions, in the North and South Range respectively, with localization of strain in a km-scale system of mylonitic shear zones, e.g. the South Range Shear Zone (Fleet et al., 1987, Riller et al., 2005). The deformation of the Sudbury structure is traditionally attributed to the Penokean orogeny (1.9 – 1.8 Ga) (Boerner et al., 2000, Mukwakwami et al., 2013). However, geochronological studies at the South Range of the Sudbury structure show orogenic reworking primarily during the Yavapai (~ 1.75 Ga), Mazatzalian – Labradorian (1.7 – 1.6 Ga), and Pinwarian (1.5 – 1.4 Ga) events (Davidson et al., 1992, Bailey et al., 2004, Papapavlou et al., 2017, Papapavlou et al., 2018).

Figure 1

The Vredefort impact structure

The Vredefort structure (South Africa) represents the oldest, largest, and most deeply eroded terrestrial impact crater (Gibson and Reimold, 2001). It is a product of collision between a < 15 km bolide impactor (Ivanov, 2005) and the Archean Kaapvaal craton, producing a ~ 250 – 300 km diameter impact structure at 2020 ± 3 Ma (Kamo et al., 1996, Moser, 1997). The central uplift of the crater consists of a core of Archean plutonic and metaplutonic units surrounded by a semicircular collar of Archean and Proterozoic supracrustal strata (**Fig. 1B**). The basement gneisses from the central uplift show ages between 3.4 – 3.1 Ga with a granulite-facies event

recorded in these rocks at 3107 ± 9 Ma (Hart et al., 1999). The two major pre-impact tectonothermal events that affected the Kaapvaal craton are the Ventersdorp event at 2.72 – 2.69 Ga and the Bushveld magmatic event at 2.06 – 2.05 Ga (Schmitz and Bowring., 2003, Graham et al., 2005). The post-impact tectonic modification of the marginal parts of Vredefort structure has been attributed to the Eburnian (2 – 1.7 Ga) and Kibaran (1.2 – 1 Ga) accretionary events (Henkel and Reimold.,1998).

Sample description

Three titanite-bearing samples, have been selected for this study; one from the North Range of Sudbury, one from the South Range of Sudbury, and one from the Vredefort structure. The North Range sample (JD12SUD13) belongs to the Levack Gneiss complex and is located approximately 600 m north of the Sudbury melt sheet (46°36'21.90"N, 81°30'52.30"W; **Fig. 1A**). Zircon grains with microtwins in adjacent felsic lithologies and baddeleyite microstructural and isotopic analysis indicates that the sample underwent impact-induced pressure and temperature conditions of P ~ 20 Gpa and T < 1000°C, respectively (White et al., 2018). The greenschist facies overprinting in the North Range of the Sudbury structure resulted in the following assemblage on the selected sample: Qtz-Chl-Fls-Act-Ep-Ttn±Zr±Ap.

The South Range sample (KPCM09), from the Creighton Mine, is a strongly foliated pseudotachylite that was retrieved from the borehole 1311300 at a depth of 2400 m and intersects with the east-west trending "Return Air Raise (RAR)" shear zone (**electronic supplementary material file 1**). The core logging shows that the foliated pseudotachylite has a thickness of ~ 4.5 m, hosts metagabbroic and felsic clasts, and abundant quartz and carbonate veinlets. The sheared pseudotachylite is passing marginally to brecciated metagabbro and diabase dykes,possibly related with the Matachewan dyke swarm (~ 2.45 Ga; Bleeker and Ernst., 2006), and to more felsic granitic intervals related with the Creighton pluton granite (~ 2.33 Ga, Frarey et al., 1982).

The sample is located at 46°28'36.40"N, 81°11'43.90"W (**Fig. 1A**). Based on 3D models, that were constructed by correlation of drillcore data, the South Range sample occurs ~ 150 m from the base of the melt sheet (personal communication with Vale). The sample from the South Range of Sudbury structure contains the most proximal titanite grains investigated to the base of the melt sheet. This sample is exposed at the low strain domains of the RAR shear zone and underwent epidote-amphibolite facies conditions that resulted in the assemblage: Hbl-Bt-Pl-Ep-Kfs-Qtz-Ttn-Ap±Zr±Ilm±Aln. The sample shows alternating biotite and amphibole-

rich bands with a strong shape preferred orientation of both amphibole and biotite grains. Within the examined specimen, BSE imaging revealed zircon grains with patchy zoning and planar microstructures (**electronic supplementary material file 2**).

The sample chosen from the Vredefort structure (**Fig. 1B**) is a titanite-bearing Archean syenogranite outcropping in a large (~100 m) exposure on the Skietkop farm (26° 58' 54.59"S, 27° 32' 59.50"E), at a radial distance of ~7 km from the geographic center of the impact. It is situated at the edge of the impact-generated thermal metamorphic aureole in a zone where quartz shock microstructures are partially recrystallized (Grieve, 1990) and zircon grains do not exhibit strong Pb-loss due to the impact event (Moser et al., 2011). Based on numerical models of the impact (Ivanov et al., 2005) the selected sample was located between the 800 and 900°C isotherms. The distance of the sample from the base of the Vredefort melt sheet is not known because the melt sheet has been removed by erosion.

Methodology

Backscatter and Forescatter electron beam imaging

Titanite grains, from the two selected samples of the Sudbury structure, were detected in-situ on reflected light maps of polished thin and thick sections. The grains from the Vredefort sample were detected following gravitational and magnetic separation and then were mounted in epoxy resin. The detected grains from Sudbury and Vredefort craters were imaged using backscatter and forescatter electron microscopy (BSE-FSE) at the University of Portsmouth using a Zeiss EVO MA 10, a Philips XL 30 CP, and a JEOL 6060 LV scanning electron microscope (accelerating voltage = 15 – 20 kV). The BSE imaging of the titanite grains was performed in high contrast and low brightness mode in order to enhance zoning defined by mean atomic number variations. FSE or orientation contrast imaging, provides a qualitative means to recognize intragrain variations in crystallographic orientation (Prior et al., 1999), and was performed only in titanite grains from the Vredefort structure using the Zeiss EVO MA 10 SEM equipped with two forescatter detectors. The FSE imaging of Vredefort grains assisted the selection of grains for the targeted microanalysis of specific intragrain domains via Electron Backscatter Diffraction mapping.

Electron Backscatter Diffraction (EBSD)

Quantitative microstructural data from titanite grains were collected using a Hitachi SU6600 FEG (Field Emission Gun) scanning electron microscope (SEM) at the ZAPLab, Western University, and a Zeiss EVO MA10 LaB_6 SEM at the University of Portsmouth. Both SEMs are equipped with an Oxford instrument Nordlys EBSD detector. Analytical details of data collection are provided in **electronic supplementary material file 3**. The crystallographic data sets were processed using the Tango (orientation map display and manipulation) and Mambo (pole figure and inverse pole figure) components of the HKL channel 5 software (Oxfords instruments). The only noise reduction operation that was applied to the raw crystallographic data was a 'wild-spike' correction that replaces isolated, erroneously-indexed pixels with zero solutions. The produced composite EBSD maps contain the following orientation components: (a) band contrast, (b) texture component, and (c) grain boundary component. The band contrast component depicts in grey scale the quality of the diffraction pattern, with darker domains denoting lower quality patterns (e.g. grain boundaries) and vice versa. Generally, the factors that influence the quality of the pattern are the: (a) diffraction intensity of the phase, (b) crystallinity in the interaction volume of the beam, and (c) crystallographic orientation (Maitland and Sitzman., 2006). Despite that the pattern quality per se does not depend on crystallographic orientation, the band contrast as monitor of pattern quality, is sensitive to crystallographic orientation because is inherently related with the visible bands of the collected electron back-scatter patterns (EBSP). Regarding the other orientation microscopy components, the colour of each pixel in the misorientation map corresponds to the minimum misorientation (i.e. disorientation) relative to a user defined reference orientation; where the interpixel orientation variation is higher than the user defined minimum, the software classifies the pixel as a grain boundary (Maitland and Sitzman., 2006). In this contribution, grain boundaries with misorientation values between 2°–10° are considered as low-angle grain boundaries whereas those with misorientations above 10° are considered as high-angle grain boundaries. In addition, as planar microstructures in the text are described the features that show 1° to 2° of misorientation in misorientation profiles whereas as microtwins the crystallographic features that show consistently misorientation angle of 74°.Is important to note also that in the examined titanite grains, the poles of the {001} crystallographic planes are parallel to the <102> direction (see also **electronic supplementary material file 6**) with the latter regarded as the disorientation axis in the angle/axis orientation descriptor reported throughout the text.

Secondary Ion Mass Spectrometry (SIMS)

The U-Pb titanite isotopic data (**electronic supplementary material file 4**) were collected using a Cameca ims-1270 secondary ion mass spectrometer at the Edinburgh Ion Microprobe Facility (EIMF). The U-Pb isotopic data were collected with a spot size of 15 μm, beam current of 6nA, and impact energy of 22keV. The U-Pb analytical session followed the sample-standard bracketing technique using Khan titanite (ID-TIMS age of 522.2 ± 2.2 Ma, Heaman, 2009) as the primary bracketing standard for the correction of instrument-induced mass fractionation. To check the accuracy and precision of the analyses the MKED1 titanite (ID-TIMS age of 1517.32 ± 0.32 Ma, Spandler et al., 2016) and Ontario – 2 titanite (LA-ICP-MS age of 1053.3 ± 3.1 Ma, Spencer et al., 2013) were used as secondary standards throughout the session. Six analyses of the MKED-1 standard yielded an upper intercept age in Wetherill concordia space of 1518 ± 11 (1σ, n = 6, MSWD = 1.16) with a weighted average $^{207}Pb/^{206}Pb$ age of 1515 ± 17 (1σ, n = 6, MSWD = 1.3). Five analyses of the Ontario – 2 secondary standard yielded a weighted average $^{207}Pb/^{206}Pb$ age of 1057 ± 67 (1σ, n = 5, MSWD = 6.5) (**electronic supplementary material file 5**). The common Pb correction was performed based on the measured $^{204}Pb/^{206}Pb$ ratios in the analysed grains and the Pb isotopic composition of modern day Pb contribution. The data were processed offline using the in-house data reduction spreadsheet used in the Edinburgh Ion Microprobe Facility and Isoplot 4.15 (Ludwig, 2003).

Results

Backscatter and forescatter electron imaging (BSE-FSE imaging)

Sudbury titanite grains (South Range)

The backscatter electron imaging of titanite grains, from the sample KPCM09, showed two main textural populations of titanite grains with different BSE signature characterised here as bright and dark BSE domains. The bright BSE domains exhibit sector zoning (**Fig. 2A)**, host one or two sets of equally spaced, parallel planar microstructures that intersect at ~ 55° and are overgrown by darker BSE domains (**Fig. 2B,** red arrows). The planar microstructures within the bright BSE domains accommodate a shearing component and displace each other.

The dark BSE domains are fractured, show patchy zoning and host apatite, ilmenite, and biotite inclusions. Fractures in the dark BSE domains stop abruptly in contact with the bright BSE domains (**Fig. 2B - 2C**). Titanite grains with dark BSE signature, that do not host bright BSE domains, define anhedral polycrystalline aggregates with patchy zoning. Within one grain (Grain 1), a bright BSE domain is overgrown by three titanite

compositional zones with darker BSE signature (**Fig. 2D**). Planar microstructures/microtwins and aligned silicate phases are observed within the two of the three overgrowth zones whereas the third zone, at the rim of the grain, shows patchy zoning and ilmenite inclusions (**Fig. 2D, white rectangle**).

Vredefort titanite grains

The examined Vredefort titanite grains show patchy zoning in BSE, with irregular slightly darker and brighter domains, and thin (<5μm) darker overgrowths (**Fig. 3A-J**). The grains are commonly fractured and show aligned trails of silicates and opaque phases. Planar microstructures are faintly recorded in BSE images (**Fig. 3B-J**) and define steps at the margin of one grain (**Fig. 3B**; red arrows). Forescatter electron imaging was performed on ten grains in order to detect the presence of planar microstructures and/or microtwins. The forescatter images are susceptible to surface topography, surface damage, and atomic number contrasts therefore further EBSD microanalysis was performed to verify the presence of these planar microstructures/microtwins. The features indicative of microtwins in FSE images, have variable apparent thickness, tapering morphology, anastomosing geometry, and different crystallographic orientation relative to their host grains (**Fig. 3K and 3L**).

Figure 2

Microstructural analysis of titanite

Sudbury grains

EBSD mapping was performed in four titanite grains, with bright and dark BSE domains, in order to elucidate the microstructural relations between these two textural populations. In grain 4, the recrystallization is localised between the bright BSE domains (**Fig. 4A-4B**). These crystallites show no internal misorientation gradients feature that indicates that they are strain-free neoblasts. The recrystallized grains and the bright BSE domains exhibit darker response in band contrast maps than the host dark BSE domains. Band contrast maps of the bright BSE domains show that the planar microstructures detected in the BSE images are cross-cutting twin lamellae, named here as St1 and St2, with variable apparent thickness (~ 1 μm to 5 μm) that laterally pinch out. High-resolution EBSD mapping (step size = 100 nm) of the intragrain domain, between the bright and dark BSE domains, show that the bright BSE domains operated as barriers to the propagation of neoblasts (**Fig. 4B**). In more detail, the bright BSE domains accommodate crystal-plastic strain up to 5°–6° and their microtwins are

misorientated from the host by 74° about <102>. The twin domains also record relative internal misorientation of up to 5°–6°. Additional EBSD data acquired from one titanite grain with cross-cutting microtwins from the sample of the North Range show that the microtwins have identical twin-host disorientation relationships with that of the South Range (i.e. 74°/<102>) (**Fig. 4C and 4D**). It is worth noting that the twinned titanite grain, from the North Range, has darker BSE signature compared to the twinned, bright in BSE, grains from the South Range. In addition, EBSD mapping of the detected grain with three overgrowth zones in BSE (Grain 1; **Fig. 2D**) shows that the planar microstructures that were detected in BSE, are microtwins that developed in three of the four intragranular domains and not only in bright BSE domains (**Fig. 4E and 4F**). The rim domain of the Grain 1 is the only domain without microtwins or planar microstructures and shows development of strain-free neoblasts (**Fig. 4F**).

Figure 3

Vredefort grains

Misorientation and band contrast maps show that three Vredefort grains (Grain 6, Grain 8, and Grain 15) host planar - curviplanar microstructures and microtwins (**Fig. 5A to 5F**). High resolution mapping (i.e. 80 nm step size) of the Grain 6 shows the nucleation of crystallites at the expense of microtwins (**Fig. 5D**). These twin-related crystallites are bounded by high (>10°) and low-angle (2–10°) grain boundaries, deviate in orientation from their parent microtwin (**Fig. 5G**), follow great circle distribution in the pole figures (e.g. {010} pole figure; **electronic supplementary material file 6**), and show no evidence of internal misorientation gradients. The parent microtwins show consistently, relative to the host, disorientation relationship of 74°/<102>, as reported from the examined Sudbury grains.

U-Pb titanite geochronology

Sudbury grains (South Range)

Six titanite grains from the sample of the South Range, that hosts both bright BSE domains and dark in BSE overgrowths, were selected for microstructurally-targeted U-Pb isotopic dating. The bright BSE domains contain up to 87 ppm U and have average Th/U ratios of 0.95. Altogether, 11 analyses were performed, with nine of them on bright BSE domains, and two analyses on dark in BSE overgrowths. Six of the nine analyses were located onto intragranular domains of bright BSE domains with planar microstructures or microtwins and three analyses onto domains with sector zoning and no deformation features in BSE images (**Fig. 2A**). The nine analyses yielded a weighted average $^{207}Pb/^{206}Pb$ date of 1851 ± 12 Ma (2σ, n = 9, MSWD = 0.76) (**Fig. 6A**) and in Wetherill concordia space a regressed upper intercept date of 1845 ± 14 Ma (2σ, n = 9, MSWD = 2.8) (**Fig. 6B**). The three analyses onto bright BSE domains with no deformation features yielded a weighted average $^{207}Pb/^{206}Pb$ date of 1848 ± 38 Ma (2σ, n = 3, MSWD = 2.5). The two analyses (i.e. analyses 2-1 and 3-1) onto the dark in BSE, locally recrystallized domains (**Fig. 2C-2D**), show extremely low U (i.e. ~1 ppm) and high common Pb contents (f206% = 15.5% and 33.2%) yielding imprecise age data. However, complementary U-Pb analyses on a larger number of grains of this low U textural population, using laser ablation - inductively coupled plasma - mass spectrometry (LA-ICP-MS) yielded a lower intercept $^{238}U/^{206}Pb$ date of 1730 ± 66 Ma (2σ, n=40, MSWD = 2.2) (Papapavlou et al., 2018).

Figure 4

Vredefort grains

Seven grains from the Vredefort structure, with planar microstructures and twin lamellae, were selected for U-Pb geochronology. Totally, 16 analyses were performed on different microstructural domains of the Vredefort grains (**Fig. 3A to 3J**). Two analyses (analyses 15.1 and 2.2) with high common Pb contents (f206% = 24% and 30.7%) were rejected and not taken into consideration on the interpretation of the data. The analysed grains have relatively low concentrations of U (average 15 ppm) and 12 of them have average Th/U of 7.4. Two analyses that are located on recrystallized twins (Grain 6) have elevated U contents (26 ppm) and lower Th/U ratios (Th/U ~ 2) compared to the population average. The U-Pb isotopic analyses yield a weighted average $^{207}Pb/^{206}Pb$ error-age of 2620 ± 24 Ma (2σ, n = 14, MSWD = 20) (**Fig. 6C**). In Wetherill concordia space the Vredefort titanites show a spread of $^{206}Pb/^{238}U$ dates between 2823 ± 33 Ma and 2378 ± 26 Ma defining a discordia line with an upper intercept date of 2636 ± 37 Ma (2σ, n = 14, MSWD = 6.3) (**Fig. 6D**). The three considerably younger analyses ($^{206}Pb/^{238}U$ = 2378 – 2412 Ma), noted with lighter blue ellipses (**Fig. 6D**), are spatially associated with planar microstructures and/or microtwins but are located also close to silicate inclusions. Excluding these three analyses, is produced an upper intercept U-Pb date of 2635 ± 14 Ma (2σ, n = 11, MSWD = 0.94) and a weighted average $^{207}Pb/^{206}Pb$ date of 2630 ± 15 Ma (2σ, n = 11, MSWD = 6.5). The $^{206}Pb/^{238}U$ dates are systematically younger than the $^{207}Pb/^{206}Pb$ dates apart from two reversely discordant analyses onto the domains with recrystalised microtwins (**Fig. 6D**).

Discussion

Interpretation of titanite microstructures

The role of titanite dynamic recrystallization on the U-Pb age resetting remains less well understood relative to zircon and monazite where it has been demonstrated that strain-free neoblasts record the timing of shock or tectonic deformation (Piazolo et al., 2012, Cavosie et al., 2015, Timms et al., 2017, Kenny et al., 2017, Erickson et al., 2017). In the examined titanite grains from the South Range of the Sudbury structure, the recrystallization is localized into the low U, dark in BSE, textural population of grains (**Fig. 2C**; analysis 3-1) that post-dates by 100 – 150 Ma the impact event (Papapavlou et al., 2018). Therefore, the neoblasts in the titanite grains from the South Range of the Sudbury structure cannot be the product of the shock strain path but product of recrystallization or annealing processes related with the post-impact metamorphic evolution of the impact

structure. The neoblastic crystallites though, that nucleated at the expense of microtwins in the Vredefort titanite grains (**Fig. 5D**), are possibly genetically unrelated with the neoblasts in the Sudbury grains (**Fig.4A-B**). These neoblasts in the Vredefort titanites could have similar origin with impact-age crystallites that developed at the expense of microtwins in zircons from the Vredefort structure and have been interpreted as products of post-shock heating by the enveloping norite melt (Moser et al., 2011).

In addition, the overgrowth relationships and the absolute U-Pb dating of the Sudbury titanite grains shows that the microtwins are localized onto older intragrain domains (bright in BSE domains) except of Grain 1 (**Fig. 2D and 4F**). In this grain, a single set of 74°/<102> microtwins transects three overgrowth zones with no evidence for twin development in the neoblasts (**Fig. 4F**). The outermost, dark grey in BSE, twin-bearing domain has low U contents (i.e. U = 1.3 ppm) and yields a discordant $^{206}Pb/^{238}U$ date of 1671 ± 67 Ma (1σ, spot 2-1; **Fig. 2D**). The low radiogenic and high common Pb contents of this texturally younger overgrowth zone didn't yield precise temporal constraints. Assuming though that this date signifies, within uncertainty, titanite growth would mean that the microtwin-forming event post-dates the 1.85 Ga impact event but predates the neoblast-forming event. Therefore, the strain accommodating event that could have resulted in the nucleation of 74°/<102> microtwins, in both craters, is either the modification of the crater (Kenkmann et al., 2013) or a later tectonic event corroborating similar disorientation relationships from tectonically deformed titanite grains (Bonamici et al., 2015, Bonamici, 2017 personal communication). The latter premise though, is based on the condition that the common disorientation relationship between host and twin indicates identical microstructural origin.

On another note, the different microstructural response of the twinned relative to the recrystallized domains in Sudbury denotes either generation of the twins under different strain-rate conditions, that is expected between impact-induced and tectonic deformations paths, or favorable orientation of the host grains for twinning (e.g. plagioclase, Ague et al.,1990). Independently of the causal mechanism, the EBSD mapping in the interface between twinned and neoblastic domains (**Fig. 4A and 4B**) revealed that the twin planes operated as barriers to the propagation of dislocation glide inducing strengthening of their host grains. Alternatively, the twin planes can also act as high energy boundaries facilitating the growth of neoblasts as in the case of tectonically deformed monazite grains (Erickson et al., 2015). Additionally, the slip accommodated by the microtwins (**Fig. 4B and 4D**) cannot be linked with a certain process since is a common phenomenon that accompanies twin nucleation (Christian and Mahajan., 1995).

Figure 5

Chronologic significance of the U-Pb age data

Previous tectonometamorphic studies, from the South Range of the Sudbury structure, have shown that titanite grains yielded ID-TIMS dates of 1815 ± 15 Ma and 1849 ± 6 Ma (Bailey et al., 2004, Mukwakwami et al., 2014). These studies attribute the ~ 1.81 and 1.85 Ga dates as evidence of Penokean metamorphism (1.9 – 1.8 Ga) with no evidence for Penokean magmatism in the area during this period (Davidson et al., 1992, Lightfoot, 2017). None of these studies documented growth or sector zoning, deformations twins, or planar microstructures in the dated grains. The sector zoning (**Fig. 2A**) and the relatively high U contents (Paterson and Stephens, 1992, Corfu and Stone., 1998) indicate that the bright in BSE titanite domains from the South Range of the Sudbury structure have magmatic origin. The absence though of trace element datasets from titanite grains of other impact melt sheets inhibits compositional comparisons. However, the presence of bright in BSE, sector-zoned, titanite grains of magmatic origin in the RAR shear zone, that is a reworked pseudotachylitic zone proximally to the basal contact of the Sudbury Igneous Complex (Papapavlou et al., 2018), would corroborate structural observations which show that these zones drained impact-produced melt pools (Riller et al., 2010). The alternative scenario would be that the bright in BSE titanite grains have pre-impact origin and underwent complete radiogenic Pb-loss induced by the impact heating in proximity to the melt sheet. Taking into consideration the geological setting where these grains were detected our preferred interpretation is that they have shock-induced petrogenetic origin and the $^{207}Pb/^{206}Pb$ date of 1851 ± 12 Ma records either the shock heating or the modification stage of crater formation. Importantly, the latter date agrees within uncertainty with the ID-TIMS U-Pb date of 1850 ± 3 Ma from titanite grains (South Range; Murray granite) that had been regrown or completely reset by the impact heating (Krogh et al., 1996).

In the Vredefort grains, the protolith possibly crystallized between 3.4 – 3.1 Ga (Hart et al., 1999), and underwent an ultrahigh-temperature metamorphic event (Ventersdorp event) that peaked between 2720 and 2715 Ma with retrograde metamorphism at 2690 ± 1 Ma (Schmitz and Bowring, 2003).The expected cooling ages based on Schmitz and Bowring (2003) for a phase with Pb closure temperature < 750°C, such as titanite, are 25 – 30 Ma younger than the 2690 ± 1 Ma event recorded in retrograde zircons. The upper intercept U-Pb date of 2636 ± 37 Ma in the examined titanite grains corroborate within uncertainty these estimations and is interpreted as the

cooling age of the 2.72 – 2.71 Ga Ventersdorp event despite some localised isotopic disturbance expressed by discordant dates.

Figure 6

Relationship of deformation twinning and U-Pb age resetting in titanite

Recent studies suggest that deformation twins (shock microtwins) can induce no or only partial U-Pb age resetting in zircon (Cavosie et al., 2015) whereas in titanite (tectonic twins) may act both as fast or inhibited diffusion pathways depending on the temperature and cooling rate (Bonamici et al., 2015). In this study, the U-Pb dating of different intragrain domains, from the bright in BSE textural population, with or without microtwins (**Fig. 2A-2B**), yielded dates that overlap within uncertainty at the stated precision levels, giving a weighted average $^{207}Pb/^{206}Pb$ date of ~ 1.85 Ga. The identical, within uncertainty, dates show that the titanite grains with deformation microtwins, from the South Range of the Sudbury structure, didn't experience detectable Pb diffusion along the twin planes. In comparison, in the Vredefort grains three analytical spots, that are spatially related with planar microstructures or microtwins (**Fig. 3**), show younger $^{207}Pb/^{206}Pb$ dates (i.e. 2441 Ma to 2582 Ma). These analyses (12-1,12-2,15-2; **Fig. 6**) are slightly discordant (-2.6% – -6.5%) and show elevated common Pb contents. Two reversely discordant analyses in analytical domains that are also related with planar microstructures (i.e. 6-1, 6-2; **Fig. 3E-5B**), indicate that microtwins and/or planar microstructures induced U-Pb isotopic disturbance in these domains (**Fig.6D**). For the latter analyses we assume that the discordant data are not artefacts of the presence of minute inclusions in the sputtered microanalytical volume. Importantly, we attribute the differential U-Pb isotopic response of the examined titanite grains from Sudbury and Vredefort crater primarily to their different petrogenetic origin and/or distance from the melt sheet.

Conclusions

The marriage of compositional-orientation imaging (BSE-FSE), quantitative microstructural analysis (EBSD), and high spatial resolution geochronology (SIMS) aimed in this study to enhance our understanding on the U-Pb isotopic response of titanite grains with different deformation microstructures from the two largest and oldest terrestrial impact craters by showing that:

- SIMS U-Pb dating of magmatic titanite grains with cross-cutting deformation microtwins and planar microstructures yields a $^{207}Pb/^{206}Pb$ age of 1851 ± 12 Ma, which is interpreted as the timing of shock heating or crater modification stage in the Sudbury impact structure.
- Overprinting microstructural relationships and absolute U-Pb dating indicate that deformation microtwins, with a disorientation relationship of 74° about <102>, are not diagnostic of shock metamorphism in titanite.
- Microstructural evidence of twin recrystallization is reported for first time in titanite and could be related with the post-shock heating effects of the enveloping impact melt sheet in the Vredefort impact structure.
- Compositionally distinct domains, in titanite grains from the South Range of the Sudbury impact structure, exhibit different rheological response with the microtwins imposing a strain-hardening effect in their host grains (bright in BSE titanite grains).
- Titanite grains from the Vredefort impact structure, record mainly the cooling of the pre-impact, ultra-high temperature, Ventersdorp event (2.72 – 2.71 Ga) with U-Pb isotopic disturbance only in domains associated with planar microstructures and a single set of 74°/<102> microtwins.

Acknowledgements

K.P acknowledges a PhD studentship from the University of Portsmouth. Vale is acknowledged for access to drillcore material. Vale geologists Lisa Gibson, Colin Mecke, Clarence Pickett and Rob Pelkey are thanked for the provided information and feedback. J.D acknowledges Higher Education Innovation Fund and Researcher Development Fund grant from the University of Portsmouth. Constructive and insightful reviews by Timmons Erickson and an anonymous reviewer enhanced the manuscript and are greatly appreciated. Previous reviews by Nick Timms, Chloe Bonamici, Fred Jourdan, and Elizaveta Kovaleva are also greatly appreciated as well as editorial handling by Steven Reddy. Personal communication with Mark Biren regarding unpublished data from the Manicouagan impact crater is also gratefully acknowledged.

References

Abramov O, Kring DA, Mojzsis SJ (2013) The impact environment of the Hadean Earth. Chemie Der Erde - Geochemistry, 73(3), 227–248 http://doiorg/101016/jchemer201308004

Ague, DM, Wenk, HR, Wenk, E (1990) Deformation Microstructures and Lattice Orientations of Plagioclase in Gabbros from Central Australia. Geophysical Monograph, 56, 173–186 http://doiorg/101029/GM056p0173

Ames, D. E., Davidson, A., Wodicka, N (2008) Geology of the giant Sudbury polymetallic mining camp, Ontario, Canda. Economic Geology, *103*(5), 1057–1077. http://doi.org/10.2113/gsecongeo.103.5.1057

Bailey, J, Lafrance, B, McDonald, A M, Fedorowich, J S, Kamo, S, WJ Davis, D A A (2004) Mazatzal–Labradorian-age (17–16 Ga) ductile deformation of the South Range Sudbury impact structure at the Thayer Lindsley mine, Ontario. Canadian Journal of Earth Sciences , 41(12), 1491–1505 http://doiorg/101139/e04-098

Biren, M, Spray JG (2010) Shock veins in the central uplift of the Manicouagan impact structure. In: 41st Lunar and Planetary Science Conference, March 1-5, Texas

Biren, M B, Spray, J G (2011) Shock veins in the central uplift of the Manicouagan impact structure: Context and genesis. Earth and Planetary Science Letters, 303(3–4), 310–322 http://doiorg/101016/jepsl201101003

Bleeker, W., Ernst, R.E (2006). Short-lived mantle generated magmatic events and their dyke swarms: the key unlocking Earth's paleogeographic record back to 2.6 Ga. In: E. Hanski, S. Mertanen, T. Ram o, J. Vuollo (Eds.), Dyke ¨ Swams—Time Markers of Crustal Evolution. Taylor and Francis/Balkema, London, pp. 3–26.

Bonamici, C E, Fanning, C M, Kozdon, R, Fournelle, J H, Valley, J W (2015) Combined oxygen-isotope and U-Pb zoning studies of titanite: New criteria for age preservation. Chemical Geology, 398, 70–84 http://doiorg/101016/jchemgeo201502002

Bonamici, C E, Kozdon, R, Ushikubo, T, Valley, J W (2014) Intragrain oxygen isotope zoning in titanite by SIMS: Cooling rates and fluid infiltration along the Carthage-Colton Mylonite Zone, Adirondack Mountains, NY, USA. Journal of Metamorphic Geology, 32(1), 71–92 http://doiorg/101111/jmg12059

Borg, I Y (1970) Mechanical <110> twinning in shocked sphene. American Mineralogist, vol 55, 1876-1888

Borg, I Y, Heard, H C (1972) Mechanical Twinning in Sphene at 8 Kbar, 25° to 500°C. Geological Society of America Memoirs, 132, 585–592 http://doiorg/101130/MEM132-p585

Cavosie, A J, Erickson, T M, Timms, N E, Reddy, S M, Talavera, C, Montalvo, S D, … Moser, D (2015) A terrestrial perspective on using ex situ shocked zircons to date lunar impacts. Geology, 43(11), 999–1002 http://doiorg/101130/G370591

Cherniak, D J (1993) Lead diffusion in titanite and preliminary results on the effects of radiation damage on Pb transport. Chemical Geology, 110(1–3), 177–194 http://doiorg/101016/0009-2541(93)90253-F

Cherniak, D, Watson, E (2001) Pb diffusion in zircon. Chemical Geology, 172(1–2), 5–24 http://doiorg/101016/S0009-2541(00)00233-3

Christian, J W, Mahajan, S (1995) Deformation twinning. Progress in Materials Science http://doiorg/101016/0079-6425(94)00007-7

Corfu, F., & Stone, D (1998) The significance of titanite and apatite U-Pb ages: Constraints for the post-magmatic thermal-hydrothermal evolution of a batholithic complex, Berens River area, northwestern Superior Province, Canada. Geochimica et Cosmochimica Acta, 62(17), 2979–2995. http://doi.org/10.1016/S0016-7037(98)00225-7

Davidson, A., van Breemen, O., and Sullivan, R.W., 1992, Circa 1.75 Ga ages for plutonic rocks from the Southern Province and adjacent Grenville Province: What is the expression of the Penokean orogeny? *in* Radiogenic Age and Isotopic Studies: Report 6, Geological Survey of Canada Paper 92-2, p. 107–118.

Darling, J R, Moser, D E, Barker, I R, Tait, K T, Chamberlain, K R, Schmitt, A K, Hyde, B C (2016) Variable microstructural response of baddeleyite to shock metamorphism in young basaltic shergottite NWA 5298 and improved U-Pb dating of Solar System events. Earth and Planetary Science Letters, 444, 1–12 http://doiorg/101016/jepsl201603032

Deer, W A, Howie, R A, Zussman, J (1997) Rock Forming Minerals, Volume 1A: Orthosilicates The Geological Society, 2nd edition, 919.

Delaney, J S, Takeda, H, Prinz, M, Nehru, C E, Harlow, G E (1983) The nomenclature of polymict basaltic achondrites. Meteoritics, 18(2), 103–111 http://doiorg/101111/j1945-51001983tb00581x

Deutsch, A, Schärer, U (1990) Isotope systematics and shock-wave metamorphism: I U-Pb in zircon, titanite and monazite, shocked experimentally up to 59 GPa. Geochimica et Cosmochimica Acta, 54(12), 3427–3434 http://doiorg/101016/0016-7037(90)90295-V

Erickson, T. M., Pearce, M. A., Taylor, R. J. M., Timms, N. E., Clark, C., Reddy, S. M., & Buick, I. S. (2015). Deformed monazite yields high-temperature tectonic ages. Geology, 43(5), 383–386. http://doi.org/10.1130/G36533.1

Erickson, T. M., Timms, N. E., Kirkland, C. L., Tohver, E., Cavosie, A. J., Pearce, M. A., & Reddy, S. M. (2017). Shocked monazite chronometry: integrating microstructural and in situ isotopic age data for determining precise impact ages. Contributions to Mineralogy and Petrology, 172(2–3), 11. http://doi.org/10.1007/s00410-017-1328-2

Erickson, T M, Cavosie, A J, Pearce, M A, Timms, N E, & Reddy, S M (2016) Empirical constraints on shock features in monazite using shocked zircon inclusions. Geology, 44(8), 635–638 http://doiorg/101130/G379791

Fleet, M. E., Barnett, R. L., & Morris, W. A. (1987) Prograde Metamorphism of the Sudbury Igneous Complex. Canadian Mineralogist, 25, 499–514.

Frarey, M.J., Loveridge, W.D., Sullivan, R.W., 1982. A U-Pb age for the Creighton granite, Ontario. Shock Metamorphism of Natural Materials, Monography Book Corporation, Baltimore, pp. 383–412.

Frost, B R, Chamberlain, K R, Schumacher, J C (2001) Sphene (titanite): Phase relations and role as a geochronometer. Chemical Geology, 172(1–2), 131–148 http://doiorg/101016/S0009-2541(00)00240-0

Ghose, S, Ito, Y, Hatch, D (1991) Paraelectric-antiferroelectric phase transition in titanite, CaTiSiO5. Physics and Chemistry of Minerals, 17(7), 591–603 http://doiorg/101007/BF00203838

Gibson R. L, Reimold W. U (2001) The Vredefort impact structure, South Africa (The scientific evidence and a two-day excursion guide). Council for Geoscience Memoir 92. Pretoria: Council for Geoscience. 111 p

Graham, I T, De Waal, S A, Armstrong, R A (2005) New U-Pb SHRIMP zircon age for the Schurwedraai alkali granite: Implications for pre-impact development of the Vredefort Dome and extent of Bushveld magmatism, South Africa. Journal of African Earth Sciences, 43(5), 537–548 http://doiorg/101016/jjafrearsci200509009

Grieve, R A, McKay, G A, Smith, H D, Weill, D F (1975) Lunar polymict breccia 14321: a petrographic study. Geochimica et Cosmochimica Acta, 39(3) http://doiorg/101016/0016-7037(75)90193-3

Grieve, R A F, Coderre, J M, Robertson, P B, Alexopoulos, J (1990) Microscopic planar deformation features in quartz of the Vredefort structure: Anomalous but still suggestive of an impact origin. Tectonophysics, 171(1), 185–200 http://doiorg/101016/0040-1951(90)90098-S

Guan, Y B, Crozaz, G (2000) Light rare earth element enrichments in ureilites: A detailed ion microprobe study. Meteoritics & Planetary Science, 35(1), 131–144 http://doiorg/101111/j1945-51002000tb01980x

Hart, R, Moser, D, Andreoli, M (1999) Archean age for the granulite facies metamorphism near the center of the Vredefort structure, South Africa. Geology, 27(12), 1091–1094 http://doiorg/101130/0091-7613(1999)027<1091

Heaman, L M, Le Cheminant, A N (2001) Anomalous U-Pb systematics in mantle-derived baddeleyite xenocrysts from ile Bizard: Evidence for high temperature radon diffusion? Chemical Geology, 172(1–2), 77–93 http://doiorg/101016/S0009-2541(00)00237-0

Heaman, L M (2009) The application of U-Pb geochronology to mafic, ultramafic and alkaline rocks: An evaluation of three mineral standards. Chemical Geology, 261(1–2), 42–51 http://doiorg/101016/jchemgeo200810021

Henkel, H., & Reimold, W U (1998) Integrated geophysical modelling of a giant, complex impact structure: Anatomy of the Vredefort Structure, South Africa. Tectonophysics, 287(1–4), 1–20. http://doi.org/10.1016/S0040-1951(98)80058-9

549 Ivanov, B A (2005) Numerical modeling of the largest terrestrial meteorite craters. Solar System Research
550 http://doiorg/101007/s11208-005-0051-0

551 Kamo, S. L., Reimold, W. U., Krogh, T. E., & Colliston, W. P (1996) A 2.023 Ga age for the Vredefort impact
552 event and a first report of shock metamorphosed zircons in pseudotachylitic breccias and Granophyre. Earth and
553 Planetary Science Letters, 144(3), 369–387. http://dx.doi.org/10.1016/S0012-821X(96)00180-X
554

555 Kenkmann, T., Collins, G. S., & Wünnemann, K (2013) The Modification Stage of Crater Formation. In Impact
556 Cratering (pp. 60–75). Chichester, UK: John Wiley & Sons, Ltd. http://doi.org/10.1002/9781118447307.ch5
557

558 Kenny, G. G., Morales, L. F., Whitehouse, M. J., Petrus, J. A., & Kamber, B. S (2017) The formation of large
559 neoblasts in shocked zircon and their utility in dating impacts. Geology, 45(11), 1003–1006.
560 http://doi.org/10.1130/G39328.1
561

562 Krogh, TE, Davis, DW Corfu, F 1984 Precise U-Pb zircon and baddeleyite ages for the Sudbury area In The
563 Geology and Ore Deposits of the Sudbury Structure. Edited by EG Pye, AJ Naldrett and PE Gilbin Special Volume
564 1: 431-446, Ontario Geological Survey

565 Krogh, T. E, Kamo, S. L, & Bohor, B. F. (1995). Shock metamorphosed zircons with correlated U-Pb discordance
566 and melt rocks with concordant protolith ages indicate an impact origin for the sudbury structure. In *Geophysical*
567 *Monograph Series*. http://doi.org/10.1029/GM095p0343
568

569 Kunz, M., Xirouchakis, D., Lindsley, D. H., & Hausermann, D. (1996) High-pressure phase transition in titanite
570 (CaTiOSiO4). American Mineralogist, 81(11–12), 1527–1530. http://doi.org/10.2138/am-1996-11-1225
571

572 Langenhorst, F, Dressler, B, (2003) First observation of silicate hollandite in a terrestrial rock. In: Proceeding of
573 the Third International Conference on Large Meteorite Impacts Geological Society of America Special Paper,
574 Abstract #4046

575 Lightfoot P.C (2017) Nickel sulfide ores and impact melts: Origin of the Sudbury Igneous Complex. Elsevier,
576 Oxford

577 Ludwig, K R (2003) User's Manual for Isoplot 3.0 - A Geochronological Toolkit for Microsoft Excel. Berkeley
578 Geochronology Center Special Publication, (4), 71

579 Maitland, T., & Sitzman, S. (2007). Electron Backscatter Diffraction (EBSD) Technique and Materials
580 Characterization Examples. Scanning Microscopy for Nanotechnology: Techniques and Applications, 41–76.
581 http://doi.org/0387396209
582

583 Moser, D E (1997) Dating the shock wave and thermal imprint of the giant Vredefort impact, South Africa.
584 Geology, 25(1), 7–10 http://doiorg/101130/0091-7613(1997)025<0007:DTSWAT>23CO;2

585 Moser, D E, Cupelli, C L, Barker, I R, Flowers, R M, Bowman, J R, Wooden, J, & Hart, J R (2011) New zircon
586 shock phenomena and their use for dating and reconstruction of large impact structures revealed by electron
587 nanobeam (EBSD, CL, EDS) and isotopic U–Pb and (U–Th)/He analysis of the Vredefort dome. Canadian Journal
588 of Earth Sciences, 48(2), 117–139 http://doiorg/101139/E11-011

589 Mukwakwami, J, Lafrance, B, Lesher, C M, Tinkham, D, Rayner, N, & Ames, D (2014) Deformation,
590 metamorphism, and mobilization of Ni–Cu–PGE sulfide ores at Garson Mine, Sudbury. Mineralium Deposita,
591 49(2), 175–198 http://doiorg/101007/s00126-013-0479-y

592 Muller, W F, Franz, G (2004) Unusual deformation microstructures in garnet, titanite and clinozoisite from an
593 eclogite of the Lower Schist Cover, Tauern Window, Austria. European Journal of Mineralogy, 16(6), 939–944
594 http://doiorg/101127/0935-1221/2004/0016-0939

595 Parrish, R R (1990) U-Pb dating of monazite and its application to geological problems. Can J Earth Sci, 27,
596 1431–1450 http://doiorg/101139/e90-152

Papapavlou, K, Darling, J R, Storey, C D, Lightfoot, P C, Moser, D E, Lasalle, S (2017) Dating shear zones with plastically deformed titanite: New insights into the orogenic evolution of the Sudbury impact structure (Ontario, Canada). Precambrian Research, 291, 220–235 http://doiorg/101016/jprecamres201701007

Papapavlou, K., Darling, J. R., Lightfoot, P. C., Lasalle, S., Gibson, L., Storey, C. D., & Moser, D (2018) Polyorogenic reworking of ore-controlling shear zones at the South Range of the Sudbury impact structure: A telltale story from in situ U-Pb titanite geochronology. Terra Nova. http://doi.org/10.1111/ter.12332

Paterson, B. A., & Stephens, W. E. (1992). Kinetically induced compositional zoning in titanite: implications for accessory-phase/melt partitioning of trace elements. Contributions to Mineralogy and Petrology, 109(3), 373–385. http://doi.org/10.1007/BF00283325

Piazolo, S., Austrheim, H., & Whitehouse, M. (2012). Brittle-ductile microfabrics in naturally deformed zircon: Deformation mechanisms and consequences for U-Pb dating. *American Mineralogist*, *97*(10), 1544–1563. http://doi.org/10.2138/am.2012.3966

Prior, D. J., Mariani, E., & Wheeler, J. (2009). EBSD in the earth sciences: Applications, common practice, and challenges. In Electron Backscatter Diffraction in Materials Science (pp. 345–360). http://doi.org/10.1007/978-0-387-88136-2_26

Putnis, A, (1992) Introduction to Mineral Sciences ,Cambridge University Press, Cambridge.

Riller, U (2005) Structural characteristics of the Sudbury impact structure, Canada: Impact-induced versus orogenic deformation-A review. Meteoritics & Planetary Science, 40(11), 1723–1740 http://doiorg/101111/j1945-51002005tb00140x

Riller, U, Lieger, D, Gibson, R. L, Grieve, R. A. F, & Stöffler, D (2010). Origin of large-volume pseudotachylite in terrestrial impact structures. *Geology*, *38*(7), 619–622. http://doi.org/10.1130/G30806.1

Spandler, C, Hammerli, J, Sha, P, Hilbert-Wolf, H, Hu, Y, Roberts, E, & Schmitz, M (2016) MKED1: A new titanite standard for in situ analysis of Sm–Nd isotopes and U–Pb geochronology. Chemical Geology, 425, 110–126 http://doiorg/101016/jchemgeo201601002

Spencer, K J, Hacker, B R, Kylander-Clark, A R C, Andersen, T B, Cottle, J M, Stearns, M A, Seward, G G E (2013) Campaign-style titanite U-Pb dating by laser-ablation ICP: Implications for crustal flow, phase transformations and titanite closure. Chemical Geology, 341, 84–101 http://doiorg/101016/jchemgeo201211012

Schmitz, M D, Bowring, S A (2003) Ultrahigh-temperature metamorphism in the lower crust during Neoarchean Ventersdorp rifting and magmatism, Kaapvaal craton, southern Africa. Bulletin of the Geological Society of America, 115(5), 533–548 http://doiorg/101130/0016-7606(2003)115<0533:UMITLC>20CO;2

Stöffler, D (1972) Deformation and transformation of rock-forming minerals by natural and experimental shock processes I Behavior of minerals under shock compression. Fortschritte Der Mineralogie 49, 50 – 113

Taylor, M, Brown, GE (1976) High-temperature structural study of the $P2_1/a$ - $A2_1a$ phase transition in synthetic titanite, $CaTiSiO_5$. American Mineralogist, 61, 435-447

Timms, N. E., Erickson, T. M., Pearce, M. A., Cavosie, A. J., Schmieder, M., Tohver, E., … Wittmann, A. (2017). A pressure-temperature phase diagram for zircon at extreme conditions. Earth-Science Reviews. http://doi.org/10.1016/j.earscirev.2016.12.008

Van Soest, M C, Hodges, K V, Wartho, J A, Biren, M B, Monteleone, B D, Ramezani, J, Thompson, L M (2012) (U-Th)/He dating of terrestrial impact structures: The Manicouagan example. Geochemistry, Geophysics, Geosystems, 12(5) http://doiorg/101029/2010GC003465

Vernon, RH, (2004) A practical guide to rock microstructure, pp.606, Cambridge University Press, Cambridge

White, L. F., Darling, J. R., Moser, D. E., Cayron, C., Barker, I., Dunlop, J., & Tait, K. T. (2018). Baddeleyite as a widespread and sensitive indicator of meteorite bombardment in planetary crusts. *Geology*, *46*(8), 719–722. http://doi.org/10.1130/G45008.1

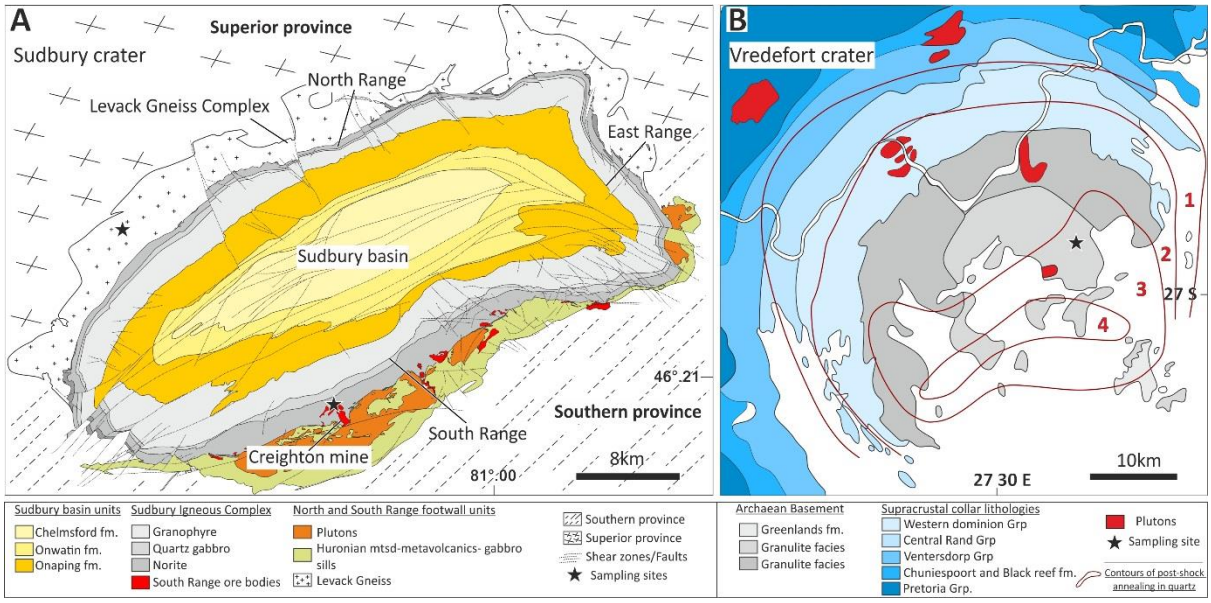

Fig. 1: Simplified geological maps of the Sudbury (A) and Vredefort impact structures (B). Black stars denote the location of the selected samples in this study. The ore bodies in the Sudbury structure are shown projected to the surface from Ames et al., 2008. The contours in Vredefort map denote the degree of post-shock thermal annealing of planar deformation features in quartz (Grieve et al., 1990); the zone 1 represents least annealing whereas the zone 4 represents complete annealing.

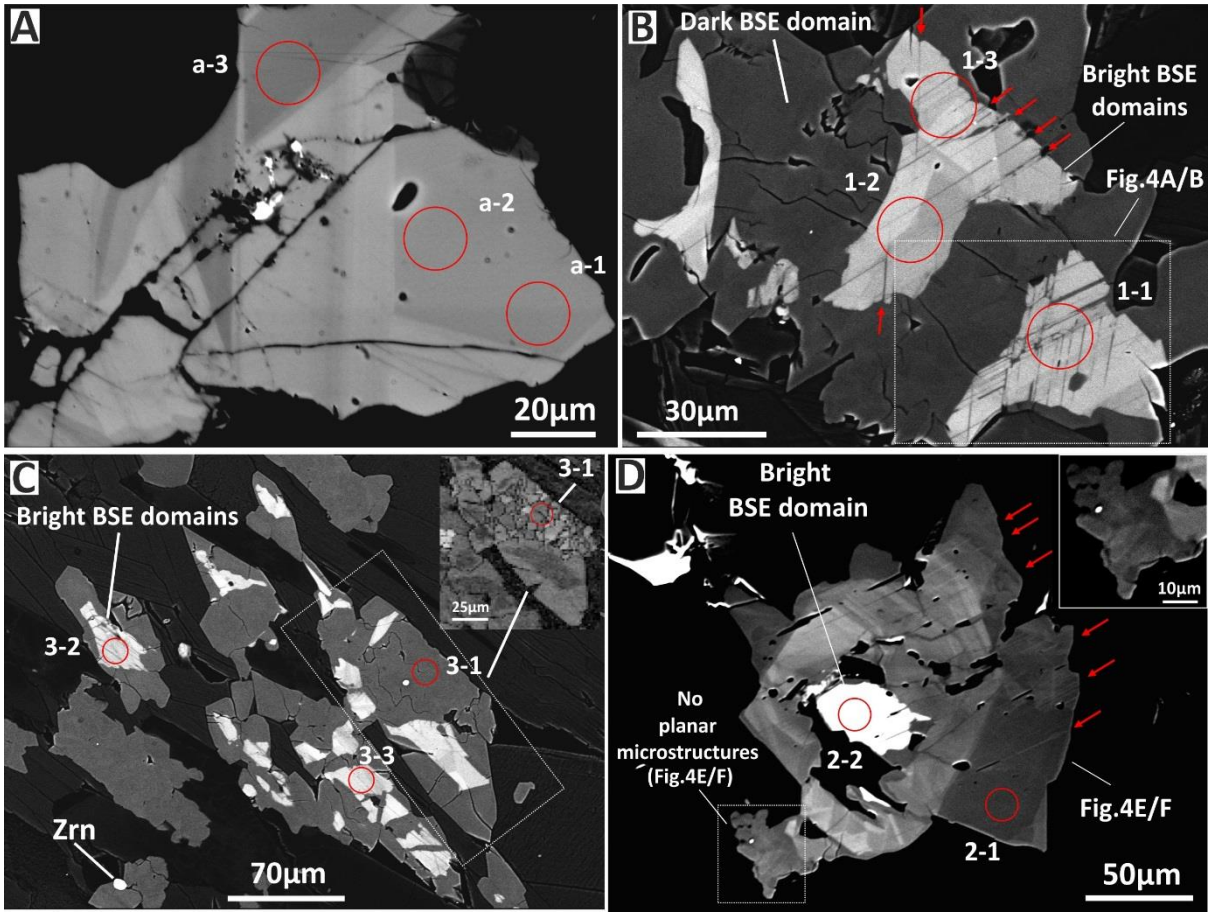

Fig. 2: Collage of backscatter (BSE) photomicrographs from the Sudbury impact structure (South Range) that depict: (A) bright in BSE titanite grain with sector zoning (Sudbury, South Range). Red circles depict the three analytical points for SIMS U-Pb microanalysis; (B) bright in BSE titanite grains with planar microstructures overgrown by darker in BSE domain. With arrows are highlighted planar microstructures/microtwins; (C) bright in BSE titanite grains with dark overgrowths. The upper right inlay of the photomicrograph shows a band contrast map of the grain in rectangle. Note that the analysis 3-1 is located in the recrystallized part of the dark overgrowth; (D) titanite grain (Grain 1, South Range; Sudbury) with multiple overgrowth zones. The planar microstructures that are highlighted with red arrows transect three of the four overgrowth zones. The upper right inlay shows the domain without planar microstructures.

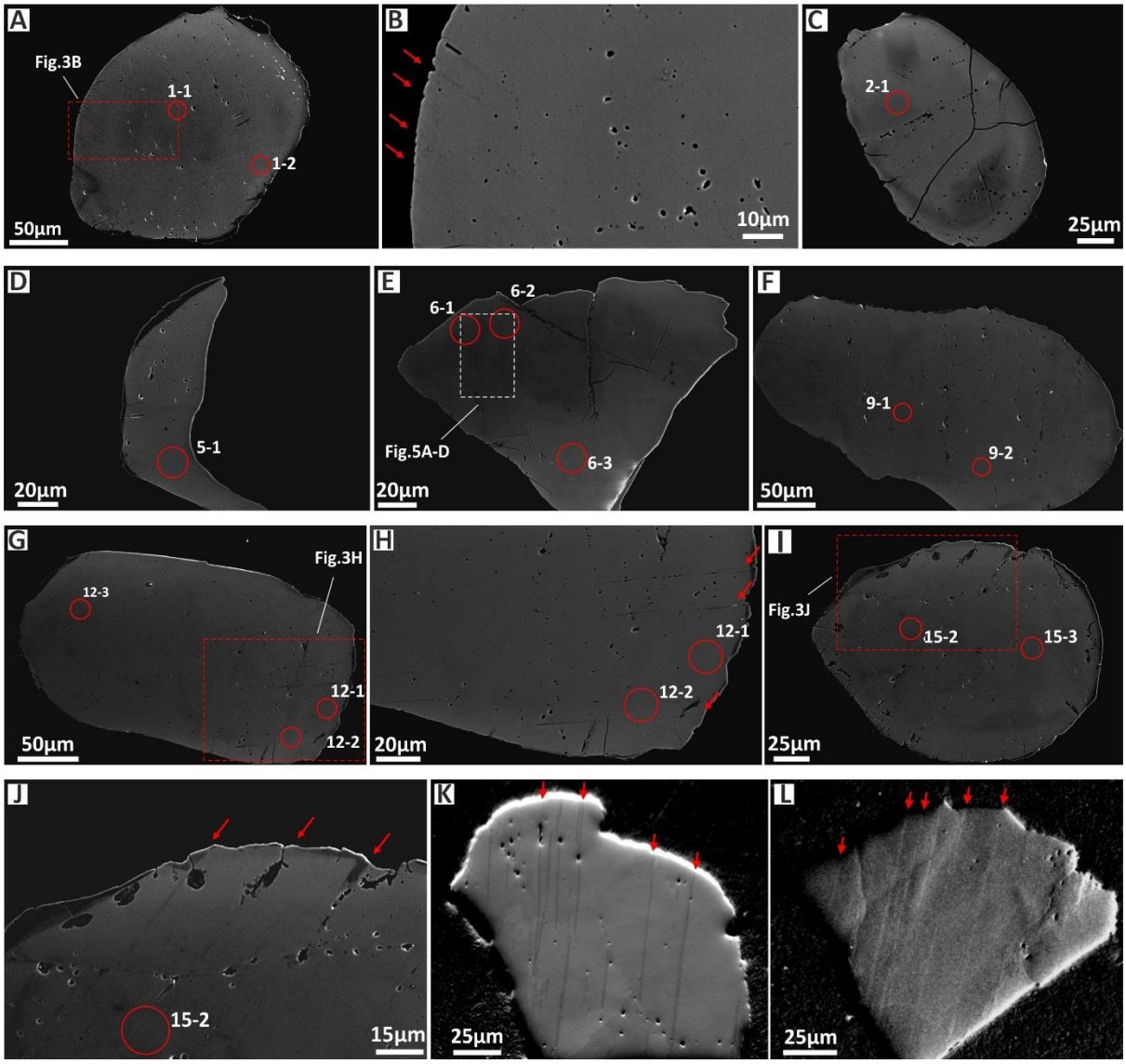

Fig. 3: Collage of backscatter and forescatter electron (BSE and FSE) photomicrographs from the Vredefort impact structure. Red circles depict the spots for SIMS U-Pb microanalysis; white rectangles mark the domains for EBSD microanalysis and red rectangles mark domains presented in higher magnification. (A-D) titanite grains with patchy zoning and planar microstructures (red arrows) from the Vredefort impact structure. Note the aligned trails of silicate phases within these grains; (E) titanite grain with patchy zoning from the Vredefort structure. Note that the U-Pb spots overlap the area for EBSD microanalysis (**Fig**. **5A-D**); (F-G) titanite grains with faint patchy zoning; (H) higher magnification BSE image of the titanite domain in red rectangle of **Fig**. **3F**. Note the presence of planar microstructures highlighted with red arrows; (I) titanite grain with faint patchy zoning. Note the parallel arrangement of planar microstructures; (J) higher magnification BSE image of the domain in red rectangle of **Fig**. **5H**. Note that the analysis 15-2 is located onto planar microstructures/microtwins; (K) FSE image of a titanite grain from the Vredefort impact structure. Note that the planar microstructures/microtwins curve and link; (L) FSE image of the titanite grain in **Fig.3E** after polishing. EBSD microstructural data from this grain are depicted in **Fig. 5** (A-D).

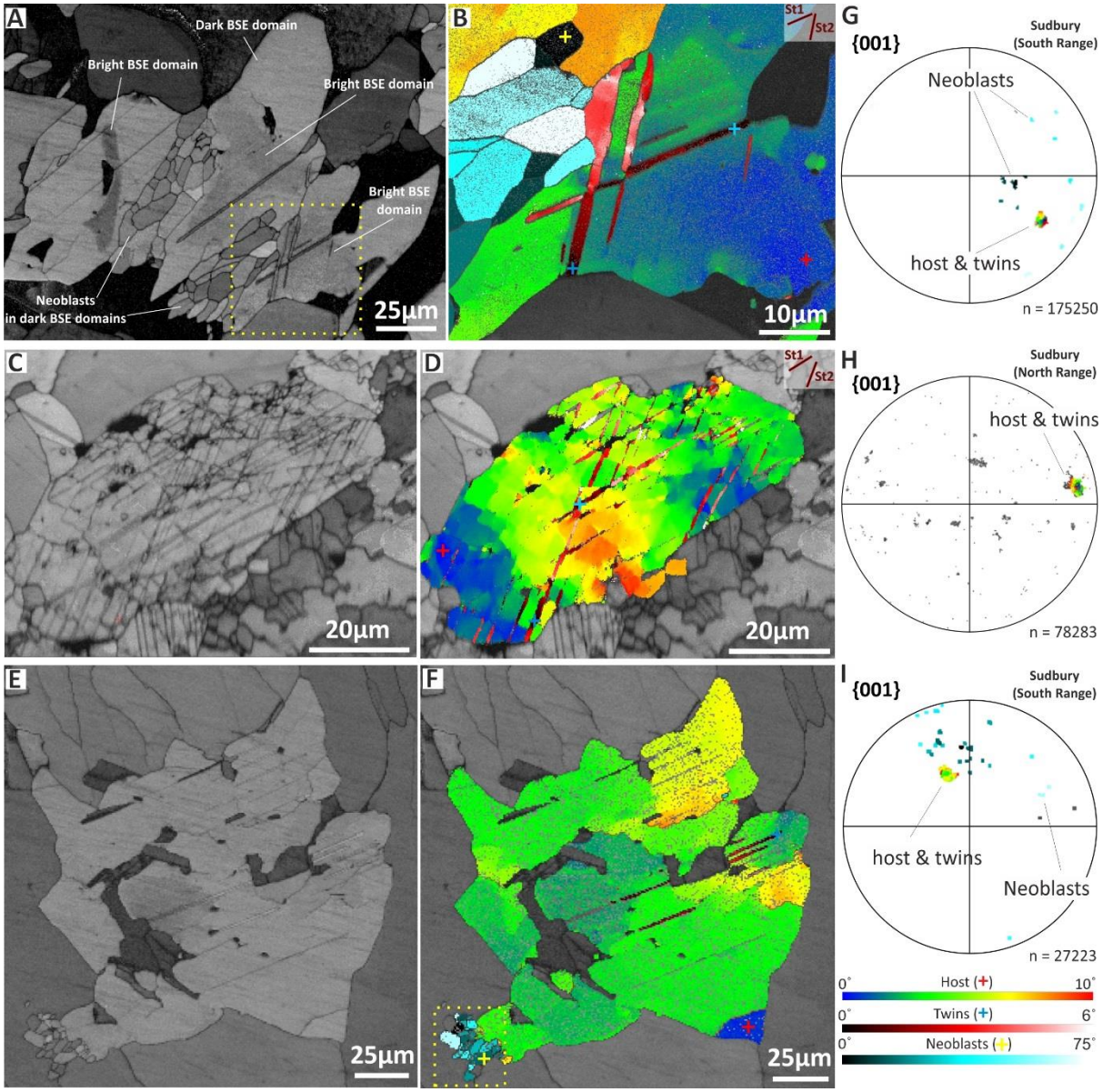

Fig. 4: Collage that shows band contrast maps (first column), misorientation maps (second column), and {001} pole figures for each EBSD map from titanite grains of the Sudbury impact structure.: (A) Band contrast map of the titanite grain depicted in **Fig. 2B**. Note that the bright grains in the band contrast map are slightly darker than the dark in BSE overgrowths. Neoblastic crystallites nucleated preferentially in domains of dark overgrowths that are located between the bright in BSE grains; (B) High resolution misorientation map of the area denoted with a yellow stitched rectangle in **Fig. 4A**. Note that recrystallization in the dark in BSE overgrowths terminates in contact with the twinned grain. In this domain the twins displace each other, have irregular geometry, and show internal deformation whereas the neoblasts don't exhibit internal deformation. With St1 and St2 are denoted the two sets of microtwins in the EBSD maps; (C) Band contrast map of a titanite grain from the North Range of the Sudbury structure; (D) Misorientation map of the North Range titanite grain; (E) Band contrast map of the titanite grain from the South Range that is depicted in the BSE image of **Fig. 2D**. Note in yellow rectangle the neoblastic domain at the rim of the grain; (F) Misorientation map of the grain that shows recrystallization only at the outermost parts; in this grain is recorded only a single set of microtwins; (G) Pole figure of the {001} crystallographic planes of the misorientation map in **Fig. 2B**.; (H) Pole figure of the {001} crystallographic planes

of the misorientation map in **Fig. 2D**; (I) Pole figure of the {001} crystallographic planes of the misorientation map in **Fig. 2F**. Note that twins and host grains share a common <102> axis (i.e. pole of the {001} planes) whereas recrystallized domains show dispersion. The colour scale at the bottom of the third column indicates the degree of misorientation relative to different reference points that are depicted with cross for different microstructural features (i.e. host grain, microtwins, neoblasts).

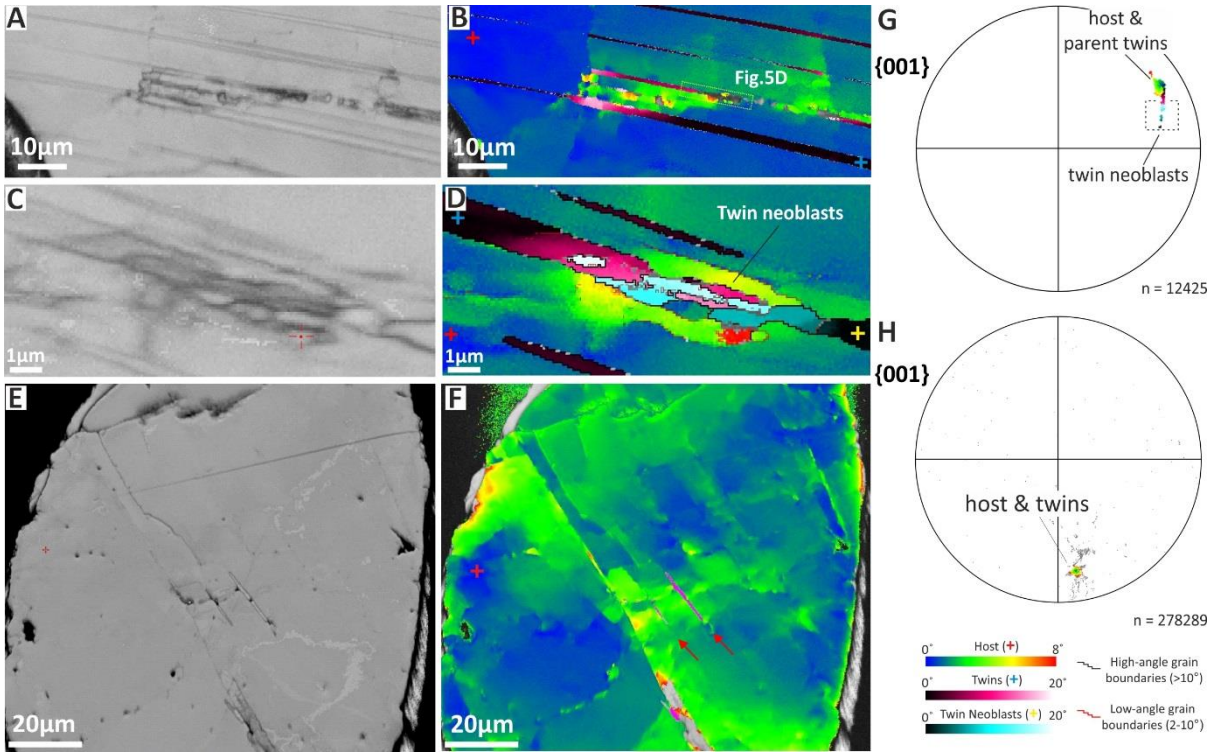

Fig. 5: Collage that shows band contrast maps (first column), misorientation maps (second column), and {001} pole figures for each EBSD map from the titanite grains of the Vredefort structure: (A) Band contrast map of the titanite grain depicted in **Fig**. **3E** (rotated anti-clockwise) that shows the presence of microtwins, (B) Misorientation map that shows that the microtwins are internally deformed up to the point of twin recrystallization (yellow parallelogram); (C) higher resolution band contrast map of the area indicated in the yellow parallelogram of **Fig. 5B**; (D) misorientation map that depicts the neoblastic crystallites bordered by high and low-angle grain boundaries; (E) Band contrast map of a titanite grain that hosts planar microstructures and microtwins; (F) Misorientation map of the **Fig. 5E** grain where is evident the presence of curvi-planar microstructures and microtwins with irregular geometry (red arrows); (G) Pole figure of the {001} crystallographic planes of the misorientation map in **Fig. 2D**. Note that twins and host grains share a common <102> axis whereas the twin neoblasts deviate in orientation from their parent twins and tend to define a great-circle distribution; (H) Pole figure of the {001} crystallographic planes of the misorientation map in **Fig. 5F**. The colour scale denotes the degree of misorientation relative to a random reference point that is depicted with cross for different microstructural features (i.e. host grain, microtwins, twin neoblasts). With black and red sawtooth lines are depicted high and low-angle grain boundaries, respectively.

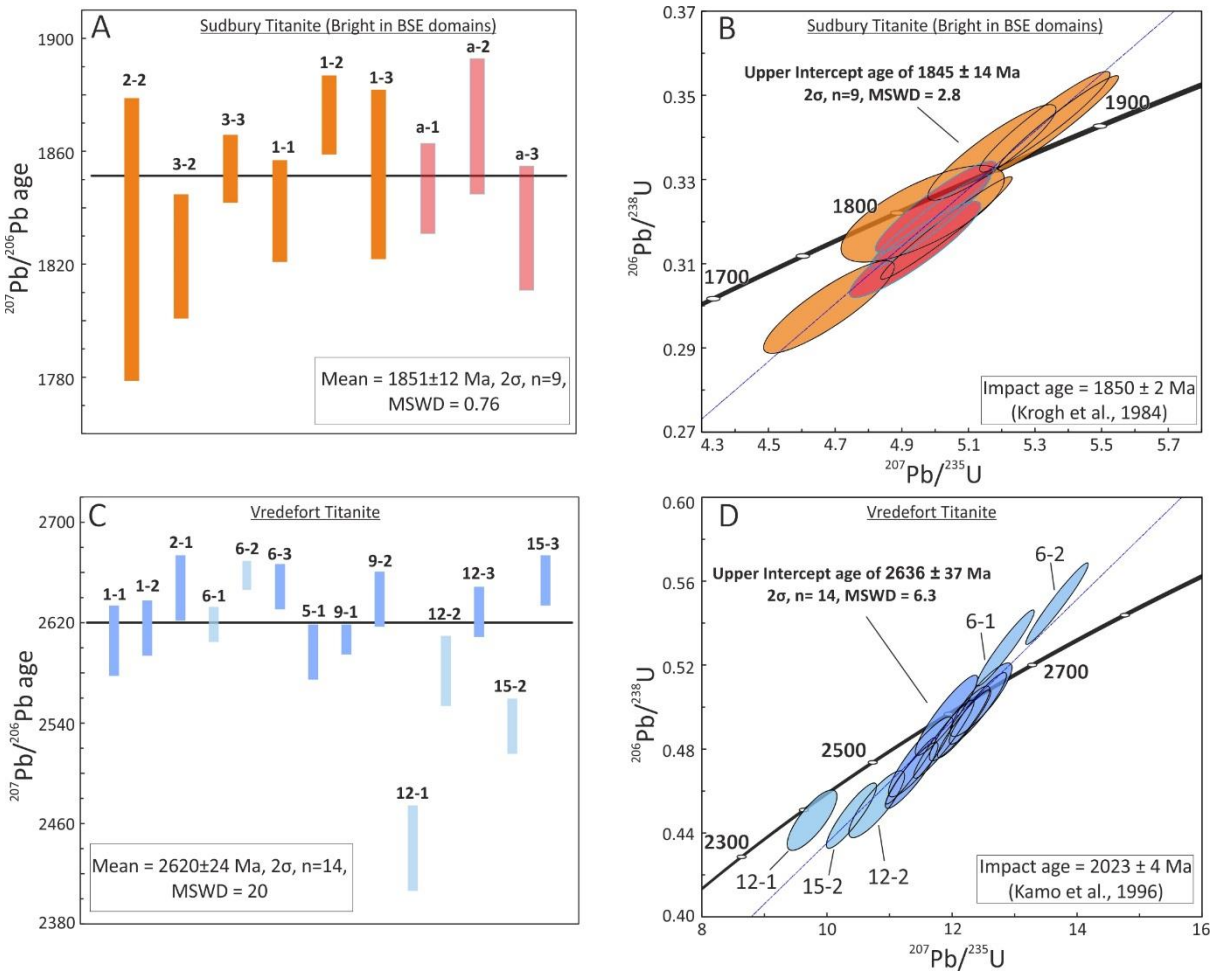

Fig. 6: U-Pb concordia and Pb-Pb diagrams from the examined titanite grains of the Sudbury and Vredefort impact structures that show: (A) $^{207}Pb/^{206}Pb$ histogram from the analysed bright in BSE titanite grains of the Sudbury structure. Pink bars denote the analyses onto intragranular domains without deformation features. With orange bars are denoted the analyses on bright intragranular domains with planar microstructures or microtwins. Above each bar is noted the analysis number; (B) U-Pb concordia diagram of bright in BSE titanite grains from the South Range of the Sudbury structure; (C) $^{207}Pb/^{206}Pb$ histogram from the examined Vredefort titanite grains. Blue bars denote the analyses onto intragranular domains without deformation features whereas light blue bars onto domains with planar microstructures or microtwins. Above each bar is noted the analysis number; (D) U-Pb concordia diagram of the analysed Vredefort grains. Note that the lighter blue ellipses denote the analyses that are associated with planar microstructures and/or microtwins (**Fig. 3**).